




Foam-lined hohlraum, inertial confinement fusion experiments on the National Ignition Facility

A. S. Moore , N. B. Meezan, J. Milovich, S. Johnson, R. Heredia , T. F. Baumann, M. Biener, S. D. Bhandarkar, H. Chen, L. Divol, N. Izumi, A. Nikroo, K. Baker, O. Jones, O. L. Landen , W. W. Hsing, and J. D. Moody
Lawrence Livermore National Laboratory, P.O. Box 808, Livermore, California 94551-0808, USA

C. A. Thomas

Laboratory for Laser Energetics, University of Rochester, Rochester, New York 14623, USA

B. Lahmann

Massachusetts Institute of Technology, Cambridge, Massachusetts 02139, USA

J. Williams, N. Alfonso, and M. E. Schoff

General Atomics, San Diego, California 92121, USA



(Received 24 August 2020; revised 9 October 2020; accepted 30 October 2020; published 19 November 2020)

Experiments on the National Ignition Facility (NIF) to study hohlraums lined with a 20-mg/cc 400- μm -thick Ta_2O_5 aerogel at full scale (hohlraum diameter = 6.72 mm) are reported. Driven with a 1.6-MJ, 450-TW laser pulse, the performance of the foam liner is diagnosed using implosion hot-spot symmetry measurements of the high-density carbon (HDC) capsule and measurement of inner beam propagation through a thin-wall 8- μm Au window in the hohlraum. Results show an improved capsule performance due to laser energy deposition further inside the hohlraum, leading to a modest increase in x-ray drive and reduced preheat due to changes in the x-ray spectrum when the foam liner is included. In addition, the outer cone bubble uniformity is improved, but the predicted improvement in inner beam propagation to improve symmetry control is not realized for this foam thickness and density.

DOI: [10.1103/PhysRevE.102.051201](https://doi.org/10.1103/PhysRevE.102.051201)

Laser-driven indirect drive inertial confinement fusion (ICF) utilizes a high-Z cavity called a hohlraum. Typically Au or U, this is used to convert directed laser energy into a uniform x-ray radiation field which can symmetrically implode a deuterium-tritium (DT) filled fusion capsule. To reach fusion conditions, the capsule must converge 20–35 times, amplifying the pressure generated and compressing the DT fuel; to achieve this, the x-ray flux asymmetry on the capsule must be <1% [1].

The time over which a hohlraum can be heated by a laser is limited by how long the laser beams can propagate inside the cavity and deposit energy. Once heated, the hohlraum begins to fill with plasma and the average electron density increases. When this exceeds the critical electron density [$n_c = 4m_e\pi^2\epsilon_0c^2/(e\lambda)^2$] for the laser wavelength (λ), the laser light can no longer propagate. In reality, the density limit at which an ICF hohlraum can be usefully driven is much lower than the critical density because as the hohlraum fills the laser deposition region moves and a capsule can no longer be driven symmetrically.

The laser beam geometry on the NIF employs four cones of 351-nm laser beams that enter a typically cylindrical hohlraum at 23°, 30°, 44.5°, and 50° relative to the hohlraum axis. The beams form two rings on the hohlraum wall, an outer cone ring where the 44.5° and 50° beams overlap close to each laser entrance hole (LEH) and an inner cone ring close to the

equator. Each end of the hohlraum is driven by 32 inner and 64 outer beams, meaning that more energy heats the outer cone region, forming a high-Z “bubble” of plasma past which the inner beams must propagate.

Experiments during the National Ignition Campaign [2,3] used a 0.96-mg/cc He gas fill to mitigate wall expansion. This led to significant backscatter from laser plasma interactions (LPI) and required the use of cross-beam energy transfer (CBET) to achieve a symmetric drive [4]; these two effects made predicting hohlraum performance difficult.

Lowering the gas-fill density [5] reduces LPI and eliminates the need to use CBET for symmetry control but allows the Au bubble to expand farther, absorbing the inner cone beams [6–9]. This limits the time during which the symmetry of the implosion can be controlled [10].

One solution to this problem is to alter the hohlraum geometry from the traditional cylinder to a range of different shapes, including “rugby” [11–13], “tetrahedral” [14–17], “ballraum” [18], “three-axis cylindrical hohlraums” [19], “I-raum,” [20] and “frustrum” [21].

Lining the hohlraum wall with foam is another approach that has been shown in simulation and experiment to reduce the wall expansion [22–24]. Foam liners tamp the isothermal expansion of the solid density hohlraum wall. Laser energy is absorbed in the foam material, resulting in a lowering of density from which the expansion originates. Experiments

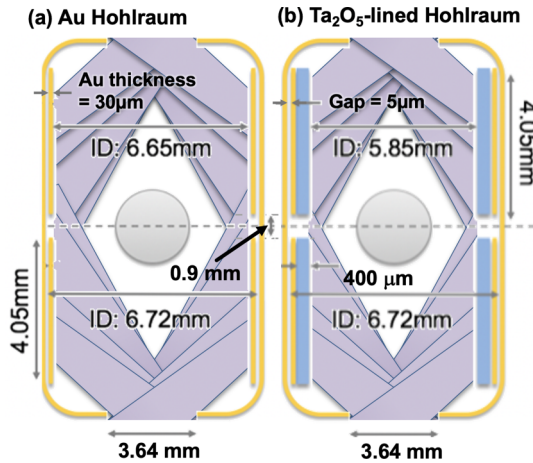


FIG. 1. Schematic of the target designs used to compare the hohlraum and capsule performance of (a) a Au hohlraum with (b) a hohlraum lined with a 20-mg/cc 400- μ m-thick Ta₂O₅ aerogel liner.

by Moore *et al.* have indicated that this reduces the electron density of the expanding plasma and should therefore improve propagation of inner-cone laser beams through the outer-cone bubble of plasma. If successful, foam liners provide an enabling technology for symmetrically driving larger capsules that absorb more energy, providing a route to higher fusion yield for the available laser energy on NIF.

We present the first ICF experiments on the NIF that measure both hohlraum and capsule performance in a careful comparison between a cylindrical Au hohlraum and one lined with Ta₂O₅ aerogel (Fig. 1). Using relative measurements of overall hohlraum temperature, capsule symmetry, implosion bang time, inner beam propagation, and wall expansion, we assess how the foam liner can improve capsule drive and symmetry.

Since laser ablation of the foam-lined hohlraum wall occurs in a lower density material, an outward-going shock is launched through the foam layer. This means that a thicker foam liner will provide a greater advantage in time. The initial hohlraum dimensions also present a geometric constraint. As the foam is made thicker, the point where the inner beams hit the foam and the capsule view of the outer beams get closer together. Eventually these points intersect and the inner-cone beams deposit energy in the same region as the outer beams,

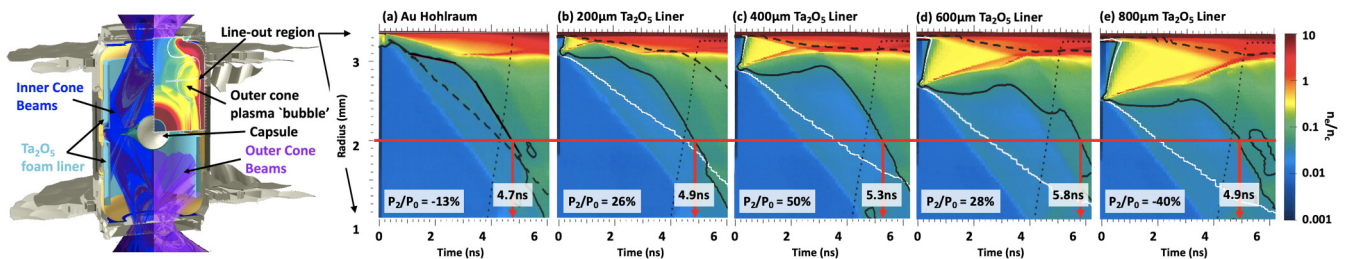


FIG. 2. Radial electron density trajectory maps from 2D HYDRA simulations for a 0.6-mg/cc He-filled “full-scale” Au hohlraum design compared to identical hohlraums lined with different thicknesses of 20-mg/cc Ta₂O₅ foam. The plots sample a radial line-out at an axial distance = 1.5 mm inside the LEH, which is centered on the bubble of plasma formed by the outer cone beams. The solid black line is $n_e/n_c = 0.04$; dashed black lines show the Au/He or Au/foam interface; white lines show the foam/He interface; and the dotted black line is the laser pulse rise to peak power. Simulated hot-spot symmetry (P_2) is annotated.

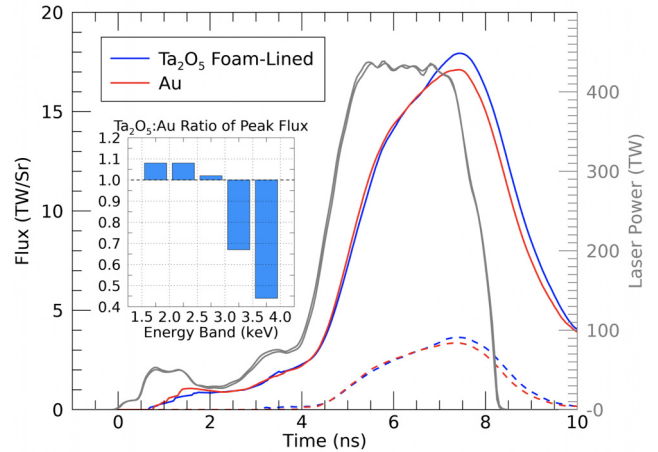


FIG. 3. The laser pulse shape for the two experiments shown in gray (leftmost lines) together with the measured x-ray flux emitted through the LEH and measured by the Dante. The x-ray flux at energies >1.8 keV is shown in dashed lines. Inset shows the ratio of peak spectra for the two cases.

resulting in an untenable asymmetric drive. Consequently, the largest full-scale ICF hohlraums that allow the use of the thickest liner should maximize the effect of the foam. The design here draws on recent low to intermediate gas-filled hohlraum experiments on the NIF [25].

Figure 2 shows the impact of foam thickness in the simulations; the radial electron density line-out through the outer bubble region of a hohlraum is shown versus time. The simulations use the pulse shape shown in gray in Fig. 3 and the high-flux model developed during the NIC [26]. Figure 2(a) is the solid Au wall case that shows the bubble expansion leading to the 4% n_c contour (solid black line) reaching a 2.0-mm radius at 4.7 ns. Simulations with increasing thicknesses of 20-mg/cc foam liner are shown in Figs. 2(b)–2(e). In these, a Ta bubble forms from the laser-heated foam, and the simulations show increasing delay in the 4% n_c contour reaching 2.0 mm of 0.2, 0.5, 1.0, and 0.2 ns respectively. The geometric limit for a 6.72-mm-diameter hohlraum is 500 μ m, so a thickness of 400 μ m was selected for the experiments from which improved beam propagation for 0.5 ns is expected. Simulation of the capsule performance for these foam parameters show a prolate implosion with P_2 symmetry of

+10% compared to an oblate implosion with $P_2 \approx -10\%$ when the foam is not present.

A nanocrystalline HDC capsule was used in each experiment; these had an inner radius of $999 \pm 1 \mu\text{m}$ and a thickness of $77.7 \pm 0.2 \mu\text{m}$ [27]. The shell included a $21\text{-}\mu\text{m}$ -thick layer of HDC doped with 0.19% W at a depth of $6 \mu\text{m}$ from the inner surface. A $5\text{-}\mu\text{m}$ fill tube was used to fill the capsule with 30:70 ratio of D : He³ to a pressure of 2500 ± 25 Torr (equivalent to a fill density of $3.20 \pm 0.03 \text{ mg/cc}$). In both cases, the hohlraum is filled with 0.3 mg/cc of He and fielded at a temperature of 40 K to reduce the He gas-fill pressure on the LEH windows. The hohlraum was driven by the laser pulse in Fig. 3 that is designed to launch three successively stronger shocks through the HDC ablator timed to converge at the inner surface of the ablator. This maximizes the rocket efficiency of the capsule while minimizing the entropy added to DT fuel, thus maximizing compression. In these experiments, there was no DT ice layer.

The foam liner was manufactured on $30\text{-}\mu\text{m}$ -thick Au rings and inserted into the open end of each half of the hohlraum prior to adding the tent and capsule. The Ta₂O₅ aerogel was cast into the 4.05-mm -long Au ring and the core removed using a laser machining technique [28,29]. To preserve the direct comparison between the Au and foam-lined experiments, the rings were also included the unlined experiment. The hohlraum also included thin-wall windows, where the $30\text{-}\mu\text{m}$ -thick Au ring is reduced to $8 \mu\text{m}$ to allow x rays $>9 \text{ keV}$ to escape while not impacting the Planckian x rays driving the capsule. [Figures 6(a) and 6(b) shows the recessed pockets and their location relative to the hohlraum.] These x rays are only produced in the direct laser-wall interaction and so the thin-wall windows provide a noninvasive way to visualize beam propagation inside the hohlraum [30].

To infer the impact of the foam liner from capsule measurements relies on the capsule x-ray drive remaining similar when the foam liner is added. Shock timing measurements were performed in separate subscale “keyhole” experiments [31] that showed the velocity of the first (28 km/s) and second (55 km/s) shocks changed by less than 0.5 km/s when the foam liner was added, but did show a 150-ps delay to the arrival of first shock. Given this small change, no adjustments were made to the pulse shape. The laser energy on this pair of shots was reproduced within $<0.5\%$, and while there was a measurable increase in backscatter when the foam liner was present, the overall coupling remained $>99\%$ (Table I).

The x-ray drive measurements in Fig. 3 were made using the Dante soft x-ray power diagnostic [32]. These show a 4% increase in the peak flux for the foam-lined hohlraum. The fraction of x rays above 1.8 keV also increased but only in line with expected from the increased temperature; however, changes to the shape of the spectrum $>1.5 \text{ keV}$ are apparent in measurements within individual channel energy ranges. Ratios of the energy in bands between 1.5 and 4.0 keV are shown in the inset to Fig. 3. These show the foam reduces energy in the band 3.0–4.0 keV while modestly increasing the flux between 1.5 and 2.5 keV. Measurements of the LEH closure [33] as a function of time indicate slightly increased closure in the foam-lined case leading to LEH diameters of $3.01 \pm 0.006 \text{ mm}$ for the Au and $2.98 \pm 0.006 \text{ mm}$ for the foam. Using these to convert x-ray flux into radiation

TABLE I. Summary of results from Au-lined (N190206-001) and Ta₂O₅-lined hohlraum (N181114-002) experiments.

	Au hohlraum	Ta ₂ O ₅ -lined hohlraum
Laser energy (kJ)	1609	1625
Backscatter (kJ)	5 (0.3%)	12 (0.7%)
Peak T_r (eV)	304.9 ± 2.3	308.9 ± 2.3
P_0 (μm)	$62.1^{+0.9}_{-0.5}$	$54.3^{+0.8}_{-2.1}$
P_2/P_0 (%)	$-10.5^{+0.2}_{-0.9}$	$-9.9^{+2.4}_{-1.5}$
$Y_n \times 10^{12}$ (DD)	0.97 ± 0.06	1.44 ± 0.06
T_{ion} (DD) (keV)	3.35 ± 0.14	3.53 ± 0.17
Fuel ρR (mg/cm ²)	78.7 ± 3.9	84.0 ± 4.8
Bang time (ns)	9.49 ± 0.04	9.50 ± 0.04

temperature, we find the 1.5% increased radiation temperature for the foam-lined hohlraum.

X-ray emission from the outer-cone bubble was imaged through the LEH. These are compared to simulation in Fig. 4 to identify the prominent features. The data on the right-hand side of the figure agree with the other LEH measurements that the LEH aperture is reduced in the foam case. Figure 4 also shows the outline of the Au bubble emission which is not azimuthally symmetric in the Au case; in fact, the radial extent of the bubble at different azimuthal angles is well correlated with the laser power. The equivalent image in the foam-lined hohlraum, in Fig. 4(b), shows no such modulation in the Ta bubble despite similar quad-to-quad power variation during the initial 2 ns of the laser pulse that determines the bubble velocity ($\pm 15\%$). The dark region in the center of each image is a measure of the plasma expansion in the LEH plane (as identified in the simulations). In the Au experiment, this is separated from the bubble position, while in the foam case the Ta bubble and Ta in the LEH plane are at similar radii. Importantly, in the foam case, the x-ray emission from high-Z material in the LEH plane is at a larger radius.

Increased x-ray drive from low-density hohlraum walls has been widely discussed and demonstrated [34,35]. The low-density foam used in these experiments results in the generation of a supersonic Marshak wave in the foam and so

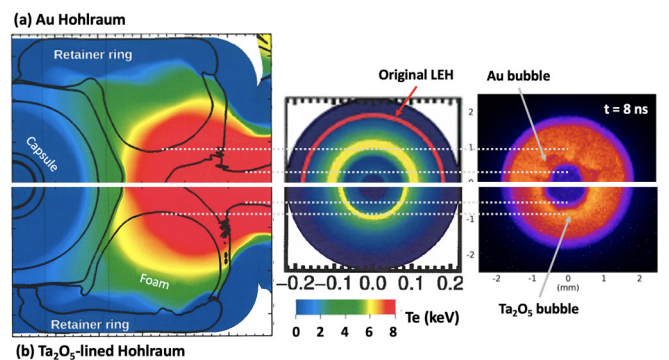


FIG. 4. Left: Simulated electron temperature inside (a) Au- and (b) Ta₂O₅-lined hohlraums. Center: Simulated x-ray emission images through the 3.64-mm LEH ($>5 \text{ keV}$) at $t = 8.0 \text{ ns}$. Right: Data at $t = 8.0 \text{ ns}$ showing reduced LEH filling and improved bubble uniformity for the foam-lined hohlraum; both images use the same color scale.

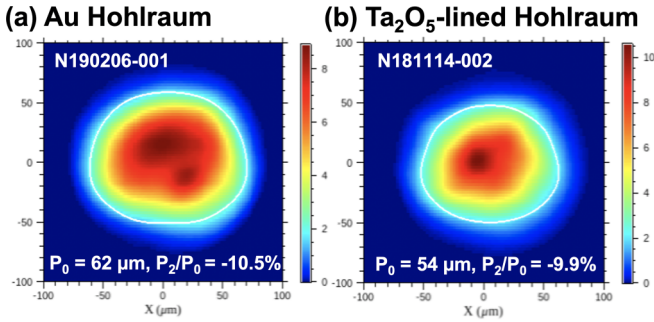


FIG. 5. The hot-spot shape is decomposed into Legendre polynomials showing oblate $P_2/P_0 \approx -10\%$ in both experiments, but a decreased average radius P_0 in the foam-lined case.

reduced wall loss would result from the density dependence of the opacity and internal energy. However, this is not the case for the 400- μm foam liner in these experiments since the Marshak wave burns through the foam in <1.0 ns. The data in the right panel of Fig. 4 provide an explanation for the improved drive in the foam experiment. Inverse Bremsstrahlung (IB) absorption scales with $\langle Z \rangle n_e^2$ [36], so a combination of less high- Z material in the LEH plane, reducing the electron density n_e , and lower average ionization $\langle Z \rangle$ of Ta₂O₅ ($\langle Z \rangle_{\text{Ta}_2\text{O}_5} \approx 20$) compared to Au ($\langle Z \rangle_{\text{Au}} \approx 50$) means that less IB occurs in the LEH plane, and when the laser propagates through the bubble the IB per unit length is lower, leading to the laser depositing energy over a greater distance and propagating further increasing the radiation temperature. This is also seen in the simulations at the equivalent time, where the volume of plasma heated to an electron temperature >5 keV is larger for the foam case. In Fig. 4(b), the bubble has expanded farther, leading to heating of the edge of the Ta bubble by the inner-cone beams, as evidenced by brighter emission on the inside edge, yet the lower average ionization of the foam leads to increased transport of the laser energy further inside the hohlraum.

Measurements of the hot-spot symmetry are shown in Fig. 5. These show both implosions are oblate by 10%. While the Au hohlraum implosion agrees with the expectation of $P_2/P_0 = -13\%$, contrary to the expectation in Fig. 2, the prolate hot spot is not realized in the foam-lined hohlraum.

The hot-spot diameter is reduced when the foam liner is added, consistent with the increased x-ray drive. The average hot-spot radius (P_0) is reduced by 12%. This is equivalent to a 33% reduction in volume, or 50% increase in pressure under the same conditions. The observed DD ion temperature was the same, meaning the DD fusion reactivity is unchanged, and so the reduction in volume is in good agreement with the 50% increase in DD neutron yield. The secondary DT neutron yield [37], increased by $\approx 60\%$ and shows improved compression, indicating the fuel ρR increased by $\approx 7\%$ from 79 to 84 mg/cm². Interestingly, while the nuclear performance improved, consistent with the reduced hot spot diameter, there was no difference in the bang time, which is suggestive of an increased implosion velocity but offset in time similar to keyhole measurements.

A simple rocket model [38] can be used to calculate the maximum implosion velocity (v_{imp}) and infer the change in

yield for x-ray drive shown in Fig. 3. Such a model predicts $v_{\text{imp}}^{\text{foam}} = 345$ km/s and $v_{\text{imp}}^{\text{Au}} = 336$ km/s.

Using this, the fuel ρR , and hot-spot radius P_0 , the yield improvement for the foam-lined symcap can be estimated as described by Hurricane *et al.*'s Eq. (20), $Y_n \sim P_0^2 (\rho R)^a v_{\text{imp}}^{2a-1}$; here $a = 3.3$. For the experiments addressed here where neither the gas temperature at peak velocity nor the measured symmetry change significantly, these terms are ignored [39]. Combining the measurements results in an estimated yield improvement of 1.64 \times , which compares favorably with the measured 1.5 \times .

One-dimensional (1D) HYDRA simulations are used to understand the improved compression observed in the secondary DT analysis. These show that for equivalent peak radiation temperatures, in 1D Y_n is increased 1.8 \times due to increased shell density in the foam-lined case compared to the Au; the increase results from changes to the x-ray drive spectrum which are also observed in the experiment (inset to Fig. 3). For the foam-lined experiment, lower energy Ta M-band radiation, generated by direct laser heating, is better shielded by the higher opacity of the HDC shell and tungsten dopant at these energies, causing a reduction in capsule preheat and higher compressibility in the foam-lined case.

Figure 6 shows >9 -keV x-ray emission measurements through a thin-wall window. The data in Figs. 6(c) and 6(d) show little difference in the emission brightness. The expectation of reduced bubble expansion due to the foam liner should lead to improved propagation of inner beams; this means emission at the equator of the hohlraum should remain bright for longer compared to the Au hohlraum experiment. This is not observed. Distinct emission regions associated with the location of quads from the upper 23 $^\circ$ and 30 $^\circ$ cones (Q33T and Q26T) are visible. Figure 6(e) shows the decrease in x-ray emission from the region associated with the inner beams. Direct comparison is nontrivial since in the Au hohlraum case emission is from the laser-heated Au L shell ($L_\alpha \approx 9.7$ keV and $L_\beta \approx 11.5$ keV), while emission from laser-heated Ta at ($L_\alpha \approx 8.1$ keV and $L_\beta \approx 9.5$ keV) is attenuated more by the 2–3 μm of unheated Au wall. Despite this complication, the emission recedes from the equator and the reduction as a function of time is consistent with the symmetry, showing no difference when the foam liner is added.

These measurements imply that the IB model used in Fig. 2 underpredicts the laser absorption. This leads the simulations to predict that laser energy can propagate through the bubble and change the implosion symmetry. The experiments show that while the laser beam propagation is improved and more energy is being deposited further inside the hohlraum, it is also due to changes in plasma filling of the LEH and is not to the extent predicted by the simulations.

Uncertainties must be considered when making assertions based on a small number of experiments. Variability in the data from each shot are reflected in the 1σ uncertainties, but repeatability from shot to shot must also be considered. A number of foam-lined hohlraums were shot at lower laser energy in the buildup to these experiments, which ensured that backscatter would not cause damage to the laser. While these are not able to reproduce the capsule performance improvement because the laser pulse was truncated, the x-ray drive measurements show repeatable performance to $<1\%$. The

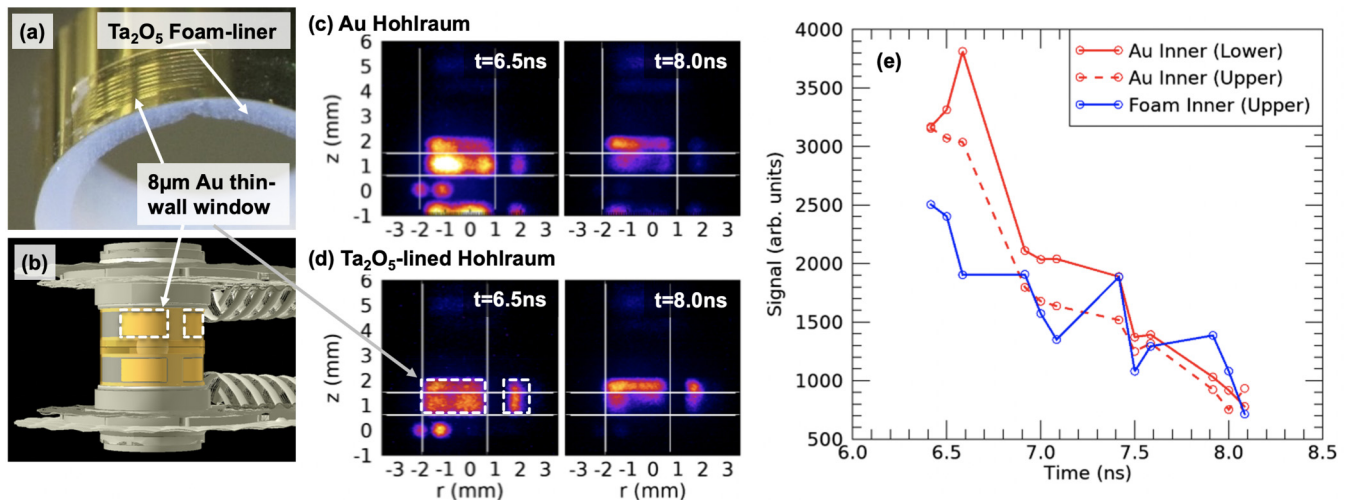


FIG. 6. Inner beam propagation is visualized using x-ray emission through thin-wall 8- μm Au pockets. (a) Photograph of foam-lined ring with milled pockets; (b) schematic of the location of the thin-wall regions as viewed by the x-ray framing camera (dashed white rectangle); (c) Au hohlraum data; and (d) foam-lined data. The two bright regions in the bottom left of each image are diagnostic windows at the hohlraum midplane for hot-spot shape measurements; the same color scale is applied to all images in panels (c) and (d). (e) Time dependence of the brightness of the inner-cone region for the Au (red and red dashed, upper) and foam-lined (blue, lower) experiments.

average density of the foam liner is measured when cast and is known to be better than 0.1%, the uniformity is characterized using radiography and indicates that local variations in density are <3% [29].

In conclusion, a pair of experiments have been performed to assess the efficacy of a 400- μm , 20-mg/cc Ta_2O_5 foam liner to improve symmetry control in an ICF hohlraum. Two-dimensional (2D) HYDRA simulations were used to guide the optimization of the hohlraum design and foam liner density and thickness. Experimental results show improved capsule performance, which is due to increased laser deposition further inside the hohlraum and changes to the x-ray drive spectrum, improving capsule compression. Together these lead to better nuclear performance in the foam-lined hohlraum. However, measurement of the inner beam

propagation and hot-spot shape both indicate that there is insufficient improvement to inner beam propagation to improve the symmetry for these foam parameters, contrary to the predictions. Given the discrepancy between simulation and experiment, future experiments will be used to test different combinations of foam density and thickness.

We are grateful O. Hurricane for useful conversations about yield scaling and for the efforts of the NIF shot operations staff for their support in developing this platform and executing the experiments. This work was performed under the auspices of the U.S. Department of Energy by Lawrence Livermore National Laboratory under Contract No. DE-AC52-07NA27344 and General Atomics under Contracts No. DE-NA0001808 and No. LLNL-JRNL-813463.

- [1] J. D. Lindl, P. Amendt, R. L. Berger, S. G. Glendinning, S. H. Glenzer, S. W. Haan, R. L. Kauffman, O. L. Landen, and L. J. Suter, *Phys. Plasmas* **11**, 339 (2004).
- [2] J. Lindl, O. Landen, J. Edwards, and E. Moses, *Phys. Plasmas* **21**, 020501 (2014).
- [3] J. D. Lindl, O. L. Landen, J. Edwards, E. I. Moses, J. Adams, P. A. Amendt, N. Antipa, P. A. Arnold, L. J. Atherton, S. Azevedo *et al.*, *Phys. Plasmas* **21**, 129902 (2014).
- [4] S. H. Glenzer, B. J. MacGowan, P. Michel, N. B. Meezan, L. J. Suter, S. N. Dixit, J. L. Kline, G. A. Kyrala, D. K. Bradley, D. A. Callahan *et al.*, *Science* **327**, 1228 (2010).
- [5] G. N. Hall, O. S. Jones, D. J. Strozzi, J. D. Moody, D. Turnbull, J. Ralph, P. A. Michel, M. Hohenberger, A. S. Moore, O. L. Landen *et al.*, *Phys. Plasmas* **24**, 052706 (2017).
- [6] P. Michel, S. H. Glenzer, L. Divol, D. K. Bradley, D. Callahan, S. Dixit, S. Glenn, D. Hinkel, R. K. Kirkwood, J. L. Kline *et al.*, *Phys. Plasmas* **17**, 056305 (2010).
- [7] A. L. Kritcher, J. Ralph, D. E. Hinkel, T. Döppner, M. Millot, D. Mariscal, R. Benedetti, D. J. Strozzi, T. Chapman, C. Goyon *et al.*, *Phys. Rev. E* **98**, 053206 (2018).
- [8] D. A. Callahan, O. A. Hurricane, J. E. Ralph, C. A. Thomas, K. L. Baker, L. R. Benedetti, L. F. Berzak Hopkins, D. T. Casey, T. Chapman *et al.*, *Phys. Plasmas* **25**, 056305 (2018).
- [9] M. B. Schneider, S. A. MacLaren, K. Widmann, N. B. Meezan, J. H. Hammer, B. E. Yoxall, P. M. Bell, D. K. Bradley, D. A. Callahan, M. J. Edwards *et al.*, *J. Phys.: Conf. Ser.* **717**, 012049 (2016).
- [10] J. E. Ralph, O. Landen, L. Divol, A. Pak, T. Ma, D. A. Callahan, A. L. Kritcher, T. Döppner, D. E. Hinkel, C. Jarrott *et al.*, *Phys. Plasmas* **25**, 082701 (2018).
- [11] M. Vandenboomgaerde, J. Bastian, A. Casner, D. Galmiche, J.-P. Jadaud, S. Laffite, S. Liberatore, G. Malinie, and F. Philippe, *Phys. Rev. Lett.* **99**, 065004 (2007).

- [12] F. Philippe, A. Casner, T. Caillaud, O. Landoas, M. C. Monteil, S. Liberatore, H. S. Park, P. Amendt, H. Robey, C. Sorce *et al.*, *Phys. Rev. Lett.* **104**, 035004 (2010).
- [13] P. Amendt, J. S. Ross, J. L. Milovich, M. Schneider, E. Storm, D. A. Callahan, D. Hinkel, B. Lasinski, D. Meeker, P. Michel *et al.*, *Phys. Plasmas* **21**, 112703 (2014).
- [14] D. W. Phillion and S. M. Pollaine, *Phys. Plasmas* **1**, 2963 (1994).
- [15] J. D. Schnittman and R. S. Craxton, *Phys. Plasmas* **3**, 3786 (1996).
- [16] J. M. Wallace, T. J. Murphy, N. D. Delamater, K. A. Klare, J. A. Oertel, G. R. Magelssen, E. L. Lindman, A. A. Hauer, P. Gobby, J. D. Schnittman *et al.*, *Phys. Rev. Lett.* **82**, 3807 (1999).
- [17] G. R. Bennett, J. M. Wallace, T. J. Murphy, R. E. Chrien, N. D. Delamater, P. L. Gobby, A. A. Hauer, K. A. Klare, J. A. Oertel, R. G. Watt *et al.*, *Phys. Plasmas* **7**, 2594 (2000).
- [18] O. S. Jones, LDRD Annual Report 2017: Advanced Fusion Target-Capsule Concepts, Tech. Rep. 15-ERD-058, Lawrence Livermore National Laboratory, 2017.
- [19] L. Kuang, H. Li, L. Jing, Z. Lin, L. Zhang, L. Li, Y. Ding, S. Jiang, J. Liu, and J. Zheng, *Sci. Rep.* **6**, 34636 (2016).
- [20] H. F. Robey, L. Berzak Hopkins, J. L. Milovich, and N. B. Meezan, *Phys. Plasmas* **25**, 012711 (2018).
- [21] P. Amendt, D. Ho, Y. Ping, V. Smalyuk, S. Khan, J. Lindl, D. Strozzi, R. Tommasini, M. Belyaev, C. Cerjan *et al.*, *Phys. Plasmas* **26**, 082707 (2019).
- [22] A. S. Moore, N. B. Meezan, C. A. Thomas, S. D. Bhandarkar, L. Divol, N. Izumi, A. Nikroo, T. F. Baumann, M. S. Rubery, J. Williams *et al.*, *Phys. Plasmas* **27**, 082706 (2020).
- [23] L. Zhang, Y. Ding, S. Jiang, J. Yang, H. Li, L. Kuang, Z. Lin, L. Jing, L. Li, B. Deng *et al.*, *Phys. Plasmas* **22**, 110703 (2015).
- [24] L. Zhang, Y. Ding, Z. Lin, H. Li, L. Jing, Z. Yuan, Z. Yang, X. Tan, L. Kuang, W. Zhang *et al.*, *Nucl. Fusion* **56**, 036006 (2016).
- [25] A. L. Kritcher, D. T. Casey, C. A. Thomas, A. B. Zylstra, M. Hohenberger, K. Baker, S. Le Pape, B. Bachmann, S. Bhandarkar, J. Biener *et al.*, *Phys. Plasmas* **27**, 052710 (2020).
- [26] M. Rosen, H. Scott, D. Hinkel, E. Williams, D. Callahan, R. Town, L. Divol, P. Michel, W. Kruer, L. Suter, R. London, J. Harte, and G. Zimmerman, *High Energy Density Phys.* **7**, 180 (2011).
- [27] J. S. Ross, D. Ho, J. Milovich, T. Döppner, J. McNaney, A. G. MacPhee, A. Hamza, J. Biener, H. F. Robey, E. L. Dewald *et al.*, *Phys. Rev. E* **91**, 021101(R) (2015).
- [28] T. F. Baumann, *Handbook of Porous Solids* (Wiley-VCH, Weinheim, Germany, 2002).
- [29] S. Bhandarkar, T. Baumann, N. Alfonso, C. Thomas, K. Baker, A. Moore, C. Larson, D. Bennett, J. Sain, and A. Nikroo, *Fusion Sci. Technol.* **73**, 194 (2018).
- [30] N. Izumi, N. B. Meezan, S. Johnson, B. N. Woodworth, T. Woods, O. S. Jones, O. L. Landen, J. J. Kroll, S. Vonhof, A. Nikroo *et al.*, *Rev. Sci. Instrum.* **89**, 10K111 (2018).
- [31] H. F. Robey, P. M. Celliers, J. L. Kline, A. J. Mackinnon, T. R. Boehly, O. L. Landen, J. H. Eggert, D. Hicks, S. Le Pape, D. R. Farley *et al.*, *Phys. Rev. Lett.* **108**, 215004 (2012).
- [32] J. L. Kline, K. Widmann, A. Warrick, R. E. Olson, C. A. Thomas, A. S. Moore, L. J. Suter, O. Landen, D. Callahan, S. Azevedo *et al.*, *Rev. Sci. Instrum.* **81**, 10E321 (2010).
- [33] H. Chen, D. T. Woods, O. S. Jones, L. R. Benedetti, E. L. Dewald, N. Izumi, S. A. MacLaren, N. B. Meezan, J. D. Moody, N. E. Palmer *et al.*, *Phys. Plasmas* **27**, 022702 (2020).
- [34] M. D. Rosen and J. H. Hammer, *Phys. Rev. E* **72**, 056403 (2005).
- [35] P. E. Young, M. D. Rosen, J. H. Hammer, W. S. Hsing, S. G. Glendinning, R. E. Turner, R. Kirkwood, J. Schein, C. Sorce, J. H. Satcher *et al.*, *Phys. Rev. Lett.* **101**, 035001 (2008).
- [36] T. W. Johnston and J. M. Dawson, *Phys. Fluids* **16**, 722 (1973).
- [37] H. G. Rinderknecht, M. J. Rosenberg, A. B. Zylstra, B. Lahmann, F. H. Séguin, J. A. Frenje, C. K. Li, M. Gatu Johnson, R. D. Petrasso, L. F. Berzak Hopkins *et al.*, *Phys. Plasmas* **22**, 082709 (2015).
- [38] D. A. Callahan, O. A. Hurricane, A. L. Kritcher, D. T. Casey, D. E. Hinkel, Y. P. Opachich, H. F. Robey, M. D. Rosen, J. S. Ross, M. S. Rubery *et al.*, *Phys. Plasmas* **27**, 072704 (2020).
- [39] O. A. Hurricane, D. T. Casey, O. Landen, A. L. Kritcher, R. Nora, P. K. Patel, J. A. Gaffney, K. D. Humbird, J. E. Field, M. K. G. Kruse, J. L. Peterson, and B. K. Spears, *Phys. Plasmas* **27**, 062704 (2020).